Applied Radiation and Isotopes 100 (2015) 16–20

Contents lists available at ScienceDirect

Applied Radiation and Isotopes

journal homepage: www.elsevier.com/locate/apradiso

Assessment of protocols in cone-beam CT with symmetric and asymmetric beams usingeffective dose and air kerma-area product

Wilson Otto Batista [a,*], Maria Rosangela Soares [b], Marcus V.L. de Oliveira [a], Ana F. Maia [b], Linda V.E. Caldas [c]

[a] Federal Institute of Bahia, IFBA, Rua Emídio dos Santos, s/n. Barbalho, CEP: 40301-015, Salvador, BA, Brazil
[b] Federal University of Sergipe, UFS, NPGFI, Rod. Marechal Rondon s/n, Jardim Rosa Elze,CEP: 49.100-000, São Cristóvão, SE, Brazi
[c] Nuclear and Energy Research Institute, IPEN, Av. Lineu Prestes 2242, Cidade Universitária, CEP: 05508-000 São Paulo, SP, Brazil

HIGHLIGHTS

- The study relies on the comparison of two image protocols in CBCT: symmetrical and asymmetrical FOV.
- Effective dose assessment for symmetrical and asymmetrical FOV.
- Measurements of *air kerma-area product* for CBCT *with* symmetrical and asymmetrical FOV.

ARTICLE INFO

Article history:
Received 30 July 2014
Received in revised form
22 November 2014
Accepted 14 January 2015
Available online 15 January 2015

Keywords:
Cone-beam computed tomography
Thermoluminescent dosimetry
Radiation protection
Radiation dosage

ABSTRACT

This study aims to evaluate and compare protocols with similar purposes in a cone beam CT scanner using thermoluminescent *dosimeter* (TLD) and the air kerma-area product (P_{KA}) as the kerma index. The measurements were performed on two protocols used to obtain an image of the maxilla–mandible using the equipment GENDEX GXCB 500: Protocol [GX1] extended diameter and asymmetric beam (14 cm × 8.5 cm-maxilla/mandible) and protocol [GX2] symmetrical beam (8.5 cm × 8.5 cm-maxillary/mandible). LiF dosimeters inserted into a female anthropomorphic phantom were used. For both protocols, the value of P_{KA} was evaluated using a PTW Diamentor E2 meter and the multimeter Radcal Rapidose system. The results obtained for the effective dose/P_{KA} were separated by protocol image. [GX1]: 44.5 μSv/478 mGy cm^2; [GX2]: 54.8 μSv/507 mGy cm^2. Although the ratio of the diameters (14 cm/8.5 cm)=1.65, the ratio of effective dose values (44.5 μSv/54.8 μSv)=0.81, that is, the effective dose of the protocol with extended diameter is 19% smaller. The P_{KA} values reveal very similar results between the two protocols. For the cases where the scanner uses an asymmetric beam to obtain images with large diameters that cover the entire face, there are advantages from the point of view of reducing the exposure of patients when compared to the use of symmetrical beam and/or to FOV images with a smaller diameter.

1. Introduction

In 1998, a new model of CT scanner was introduced worldwide and becoming an important tool for dentistry (Mozzo et al., 1998). Differing from the traditional medical scanner, which has the radiation beam in a fan-shape, these new scanners have a radiation beam with conical geometry. The first commercial model was the *NewTom-9000*, manufactured by *Quantitative Radiology* (Mozzo et al., 1998), Verona, Italy.

From this moment arises the need to introduce a metric to quantify the dosimetric point of view these exposures. The dosimetry and kerma index in tomography with a fan-shaped beam are well established with standardised phantoms. The indices of the air kerma or the weighted air kerma in computed tomography, C_a and C_w (Batista et al., 2013; IAEA, 2007) are well defined and are very useful in evaluating protocols and estimating the effective dose in medical CT scanners with fan-shaped beam (Batista et al., 2013). These measured indices are measured with the ionization chamber (pencil chamber), typically with a length of 100 mm.

The determination of the weighted air kerma index in computed tomography (C_w) uses the phantom dosimetric standard: four holes in the periphery and a central hole (Batista et al., 2013;

* Corresponding author.
E-mail address: wilsonottobatista@gmail.com (W.O. Batista).

http://dx.doi.org/10.1016/j.apradiso.2015.01.014
0969-8043/

IAEA, 2007). These simulators are suitable for dosimetry in conventional CT with a fan-shaped beam where the rotation axis is fixed, independent of the study performed.

Currently, the cone beam CT is an emerging and powerful technology in dental radiology that presents significant differences from the point of view of technological design between different manufacturers on the world market (Batista et al., 2013). Practically all existing models on the market cone beam CT have the option to change the axis of rotation according with the exam/study to be carried. This makes it unfeasible to use C_w to evaluate the radiation exposure parameter or compare techniques. Consequently, the existing dosimetric phantoms do not have the characteristics necessary to allow dosimetric measurements for cone beam CT scanners (Batista et al., 2013). For this reason, the estimates/assessments of the exposure levels in Cone Beam CT are based on thermoluminescent dosimetry (TLD) (Ludlow et al., 2006; Pauwels et al., 2014; Wu et al., 2014) and P_{KA}. Another option, with the main objective of reducing the costs associated with detectors of large dimensions, is available on some models. Thus, some models acquire images with superior physical area of the image receptor diameters. This is only possible with the displacement of the image receptor of the central position in conjunction with the use of asymmetric or off-axis beams.

This study aims to evaluate and compare protocols with similar purposes on equipment from the cone beam CT using TLDs inserted into an anthropomorphic phantom and the product of the air kerma with the area as the kerma index (P_{KA}).

2. Materials and methods

2.1. Equipment and protocols assessed

Two protocols were evaluated in a cone beam CT scanner GXCB 500 Gendex, KaVo Dental GmbH (Biberach/Riß, Germany). Fig. 1 presents the position of the simulator on scanner to perform the exposures. Table 1 presents the technical characteristics of the equipment. Measurements were taken following two protocols to obtain the image of the two dental arches, maxilla and mandible: protocol [GX1] extended diameter and asymmetric beam (14 cm × 8.5 cm-maxilla/mandible) and Protocol [GX2] symmetrical beam (8.5 cm × 8.5 cm-maxillary/mandibular).

The geometry of irradiation, symmetric and asymmetric beam for each protocol are shown in Fig. 2. The asymmetric geometry of Fig. 2(a) is obtained by shifting the detector and adjusting the beam collimators to obtain an asymmetrical x-ray beam, thus generating an image with a diameter of 14 cm (Scarfe and Farman, 2008). Under the conditions of Fig. 2(b), a symmetrical beam is used to generate an image with a diameter of 8.5 cm.

A female anthropomorphic phantom manufactured by RSD-Radiology Support Devices (Long Beach, CA-USA) was used to simulate the most approximate conditions of exposure and dose deposition in a real patient.

Table 1
Technical specifications of CBCT Gendex GXCB.

kVp	120
Focal spot	0.5
Voxel sizes	0.4 mm/0.3 mm/0.25 mm/0.2 mm/0.125 mm
Image detector	a-Si-Amorphous Silicon Flat Panel
Sensor size	13 cm × 13 cm
Resolution	14 lp/cm (voxel size 0.2 mm)
Shades of gray	16384 shades of gray – 14 bit
FOV[a]	8 × 8 cm – Standard 14 × 8 cm – EDS[b]

[a] Field of View.
[b] EDS – Extended Diameter Scan.

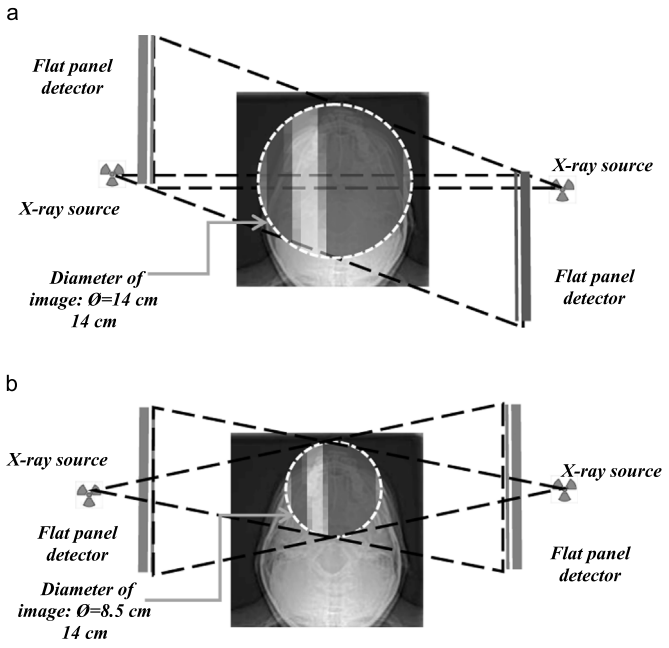

Fig. 2. Geometry for image acquisition. (a) asymmetric beam (b) symmetric beam.

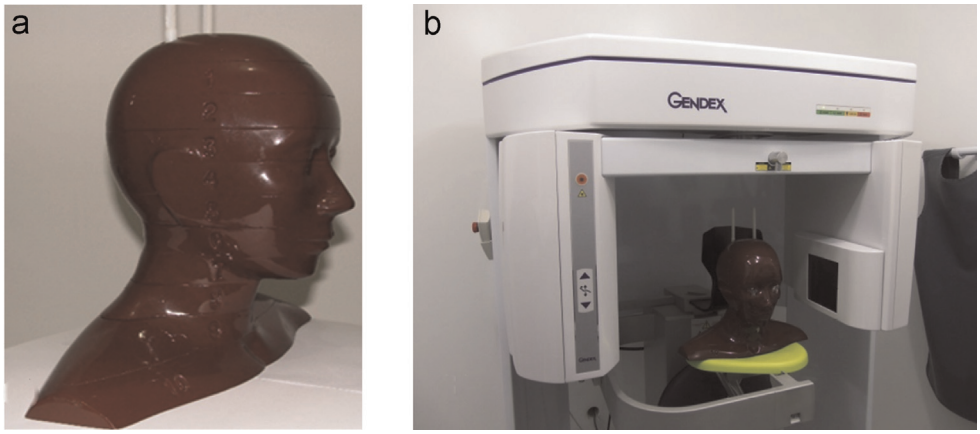

Fig. 1. (a) The female phantom RSD; (b) positioning of anthropomorphic phantom to carry out the exposures under the same conditions of clinical location.

Table 2
Distribution of dosimeters (TLDs) in the various tissues and organs the phantom.

No. *TLD*	Organ or tissue(slice)
1	Surface of the left cheek (5)*
2	Posterior neck (5)*
3	Left thyroid (8)*
4	Right lens (3)*
5	Left lens (3)*
6	Posterior calvarium (2)
7	Calvarium right (2)
8	calvarium left (2)
9	Anterior calvarium (2)
10	Midpoint of the brain (2)
11	Pituitary gland (3)
12	Right orbit (3)
13	Left orbit (3)
14	Center of the spinal spine (5)
15	Right parotid (5)
16	Right ramus (5)
17	Reft parotid (5)
18	Left ramus (5)
19	Center of the sublingual gland (6)
20	Right submandibular (6)
21	Left submandibular (6)
22	Right mandible (6)
23	Left mandible (6)
24	Esophagus (9)
25	Right thyroid (9)
26	Left thyroid (9)

* TLD placed on the surface.

2.2. Positioning of the dosimeters

Twenty-six dosimeters, TLD-100 (LiF: Mg, Ti) were used. The TLDs were inserted in the simulator, in representative positions of the structures of the head and neck (Koivisto et al., 2012; Ludlow et al., 2006) as shown in Table 2. The location of the tissues/organs was guided by experts in dental radiology. Table 2 shows the distribution of thermoluminescent dosimeters in each slice of the phantom.

2.3. Calibration, irradiation and readout of the TLDs

The dosimeters were calibrated by exposing each crystal individually, the values of known dose of 1 and 15 mGy generated by an x-ray beam with computed tomography qualities RQT 9 with a distance of 1 m between the focal point and the crystal. The equipment generating the x-rays was *Pantak/Seifert 160HS ISOVOLT* (Stone Mountain, GA, USA), installed in the Institute of Nuclear Energy Research Lab (IPEN). Energy dependence was assessed irradiating the dosimeters with 5 mGy at RQT8, RQT9 and RQT10 qualities. The measured energy dependence was 0.6% for those qualities.

The reading of the TLDs in the calibration process and the process for obtaining the dosages was performed with a Harshaw TLD reader, model QS 3500 (Waltham, MA-USA), with the support of WinREMS software coupled to a data acquisition system. The absorbed dose determined for each TLD is the result of the dose response curve, Fig. 3, obtained by considering the correction factor related to the calibration and reference light at the time of reading. The coefficient of variation of TLD was 8% and maximum uncertainty was 10%.

Three exposures were carried out for each protocol and the final value was taken to be the dosimeter reading divided by three.

2.4. Measurements of air kerma-area product

For all protocols evaluated, the value of P_{KA} was obtained using a P_{KA}-meter, PTW Diamentor E2 (Freiburg · Germany), and/or

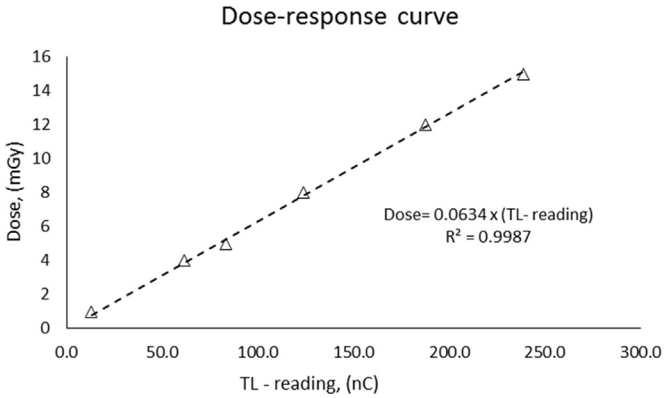

Fig. 3. Dose response curve for the range from 1 to 15 mGy.

with a solid state multimeter Rapidose, Radcal (Monrovia, CA-USA).

The transmission ion chamber was positioned in the output beam of x-rays and the multimeter positioned on the surface of the image receptor. The camera directly assesses the air kerma-area product (P_{KA}) and kerma values recorded with the multimeter, multiplied by the x-ray field area in this position, we obtained the value of $P_{KA.}$ Therefore we used two methods to assess the values of P_{KA}, thus making the results reliable.

2.5. Use of the ionization chamber Farmer

Additional measurements with a Farmer ionization chamber $10 \times 6 - 0.6$CT coupled to the multimeter Accu-Gold, Radcal (Monrovia, CA-USA), inserted in different positions within a disk of PMMA. The ionization chamber is calibrated for CT quality and energy dependence declared by the manufacturer is $\pm$ 5% in the range of 3–20 mm Al HVL.

The disk of PMMA has nine holes distributed as shown in Fig. 4. The purpose of these measurements with the ionization chamber is to demonstrate that positions close to the center are irradiated only during part of the rotation time. For clarity, Fig. 4 presents the nine position and two radiation beam geometries. The ionization chamber was positioned at the nine positions available.

2.6. Effective dose, ED

The effective dose values were obtained using Eq. (1):

$$ED = \sum_T H_T . w_T \quad (1)$$

The equivalent dose H_T being defined by

$$H_T = w_R \sum_i f_i . D_{Ti} \quad (2)$$

where w_R is the radiation weighting factor (w_R = 1 Sv/Gy for x-rays), f_i is the fraction of the slice tissue T_i that has been irradiated, D_{Ti} is the absorbed dose in tissue T_i in the slice i and w_T is the factor weight of the tissue[5,6]. The weighting factor w_T used for organs and tissues is taken from the recommendations published by the International Commission on Radiological Protection, ICRP 103 (ICRP, 2007).

3. Results

The results of P_{KA} represent averages for five measurements carried out with the ionization chamber. The values recorded through the multimeter was confronted with those obtained from

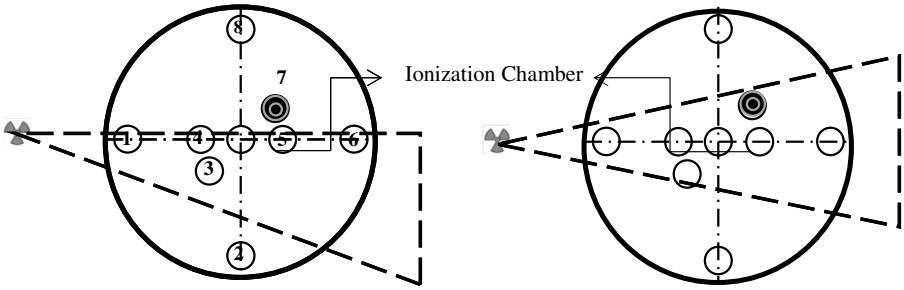

Fig. 4. Positions of measurements showing the arrangement of radiation beams and nine possible positions of the ionization chamber: (a) asymmetric geometry (b) symmetric geometry.

ionization chamber. We use only the results of the multimeter to monitor the stability of the radiation beam because the measures were simultaneous and in this configuration the measured values recorded in multimeter already has the contribution of the attenuation of the transmission chamber. However, this set of measurements was useful in reliability of results.

The results obtained for effective dose and P_{KA} are separated by protocol image. For Protocols [GX1] and [GX2] the results, presented in the Table 3, of effective dose and P_{KA} were, respectively 44.5 μSv/478 mGy cm^2 and 54.8 μSv/507 mGy cm^2. Table 4 presents the equivalent doses to the organs and tissues of the structure of the head and neck for both protocols. All positions, organs and tissues are listed in ICRP (2007), and located in the simulator was assisted by an experienced dental radiologist.

The results of measurements with the ionization chamber are shown in Table 5. The data are organized by position in the PMMA plate. These positions were chosen to represent locations of organs and tissues in the center and periphery the cross section. In this table, Table 5 is presented the kerma values for each position of the Farmer ionization chamber and also the average value of the kerma.

Table 4
Values of equivalent dose and effective dose (ICRP, 2007).

Organ/Tissues	Equivalent dose, ($\propto\Sigma\varpi$)	
	Protocol [GX1]: 14 cm × 8.5 cm	Protocol [GX2]: 8.5 cm × 8.5 cm
Salivary glands	11.3	16.3
Thyroid	7.0	6.8
Bone marrow	6.5	6.9
Bone surface	1.8	1.9
Esophagus	0.7	0.7
Brain	0.8	1.3
Skin	0.6	0.7
Remainder[a]	15.9	20.4
Lymphatic nodes	6.9	9.4
Extrathoracic airways	49.4	43.8
Muscle	6.9	9.4
Oral mucosa	143.3	202.9
Effective dose	**44.5 μSv**	**54.8 μSv**

[a] Adipose tissue, adrenals, extrathoracic (ET) region, gall bladder, heart, kidneys, lymphatic nodes, muscle, oral mucosa, pancreas, prostate, small intestine, spleen, thymus, uterus/cervix.

4. Discussion

These values indicate that although the diameter of the image acquired in the protocol [GX1] is greater than the diameter of the image in the protocol [GX2], with a ratio between the diameters of 1.65, the effective dose for the first protocol, [GX1] is lower by approximately 19%. In contrast, the values of P_{KA} show very similar results between the two protocols. Thus, although common sense would lead suggest that imaging protocols with larger field of views (FOV) would imply higher values for the effective dose than small diameters, it has been demonstrated that, in this particular case, this is not true, due to the asymmetric beam technology.

It is easy to explain why the value of the effective dose associated with the image of 14 cm of diameter is less than the value of the effective dose for an image with a diameter of 8.5 cm. In the asymmetric beam or off-axis geometry, Fig. 2(a), organs such as the salivary glands and lymph nodes remain exposed to the direct beam only part of acquisition (Morant et al., 2013). On the other hand, these organs are exposed during the entire the image acquisition time at protocols that uses symmetric beam. This is verified through the values of the equivalent dose, Table 4, in these organs derived from the two protocols [GX1]/[GX2]: the salivary glands have 11.3 μSv/16.3 μSv and the lymph nodes, 6.9 μSv/9.4 μSv. See also the data presented in Table 5, the kerma values assessed through the ionization chamber.

Table 3
Values of effective dose and air kerma-area product (P_{KA}), for both protocols.

Protocol	Effective dose, ($\propto\Sigma\varpi$)	P_{KA}, (mGy cm^2)
[GX1]: 14 cm × 8.5 cm	44.5	478
[GX2]: 8.5 cm × 8.5 cm	54.8	507

Table 5
Kerma values depending on positions in relation to the axis of rotation.

Positions	*FOV*=14 cm × 8.5 cm		*FOV*=8.5 cm × 8.5 cm	
	kerma (mGy)	Mean value (mGy)	kerma (mGy)	Mean value (mGy)
1/6	1.403/1.598	1.501	2.087/2.132	2.110
2/8	1.557/1.504	1.532	2.296/2.313	2.305
3/7	1.279/1.255	1.267	2.578/ 2.553	2.565
4/5	1.289/1.234	1.261	2.534/ 2.549	2.542
Center	2.466	–	2.532	–

5. Conclusions

The results indicate the importance of knowing the technological design and assessing the protocols available. They also indicate that for the cases where the scanner uses an asymmetric beam to obtain images with large diameters that cover the entire face, there are advantages from the point of view of reducing the exposure of patients with respect to the use of symmetrical beam and/or to FOV images with a smaller diameter.

Acknowledgments

The authors thank the Laboratory of Physical Radiology of the Federal Institute of Bahia (LAFIR/IFBA), the Institute of Nuclear Energy Research Lab (IPEN).

References

Batista, W.O., Navarro, M.V., Maia, A.F., 2013. Development of a phantom and a methodology for evaluation of depth kerma and kerma index for dental cone beam computed tomography. Radiat. Prot. Dosim. 157, 543–551.

IAEA, 2007. Dosimetry in Diagnostic Radiology: An International Code of Practice. International Atomic Energy Agency, Vienna, p. 356, Technical Reports Series No. 457.

ICRP, 2007. The 2007 Recommendations of the International Commission on Radiological Protection, ICRP publication 103, Ann ICRP. 37. pp. 1–332.

Koivisto, J., Kiljunen, T., Tapiovaara, M., Wolff, J., Kortesniemi, M., 2012. Assessment of radiation exposure in dental cone-beam computerized tomography with the use of metal-oxide semiconductor field-effect transistor (MOSFET) dosimeters and Monte Carlo simulations. Oral Surg., Oral Med., Oral Pathol. Oral Radiol. 114, 393–400.

Ludlow, J.B., Davies-Ludlow, L.E., Brooks, S.L., Howerton, W.B., 2006. Dosimetry of 3 CBCT devices for oral and maxillofacial radiology: CB Mercuray, NewTom 3G and i-CAT. Dentomaxillofacial Radiol. 35, 219–226.

Morant, J., Salvadó, M., Hernández-Girón, I., Casanovas, Ortega, R., Calzado, A., 2013. Dosimetry of a cone beam CT device for oral and maxillofacial radiology using Monte Carlo techniques and ICRP adult reference computational phantoms. Dentomaxillofacial Radiol. 42, 92555893.

Mozzo, P., Procacci, C., Tacconi, A., Martini, P.T., Andreis, I.A., 1998. A new volumetric CT machine for dental imaging based on the cone-beam technique: preliminary results. Eur. Radiol. 8, 1558–1564.

Pauwels, R., Cockmartin, L., Ivanauskaite, D., Urboniene, A., Gavala, S., Donta, C., Tsiklakis, K., Jacobs, R., Bosmans, H., Bogaerts, R., Horner, K., 2014. Estimating cancer risk from dental cone-beam CT exposures based on skin dosimetry. Phys. Med. Biol. 59, 3877–3891.

Scarfe, W.C., Farman, A.G., 2008. What is Cone-Beam CT and How Does it Work? Dent. Clin. N. Am. 52, 707–730.

Wu, J., Shih, C.-T., Ho, C.-h., Liu, Y.-L., Chang, Y.-J., Min Chao, M., Hsu, J.-T., 2014. Radiation dose evaluation of dental cone beam computed tomography using an anthropomorphic adult head phantom. Radiat. Phys. Chem. 104, 287–291.